Supplementary information

Copper Catalysed Tyrosine Nitration

Liang Qiao,[a] Yu Lu,[a] Baohong Liu,[b] Hubert H. Girault*[a]

[a] *Laboratoire d'Electrochimie Physique et Analytique, Ecole Polytechnique Fédérale de Lausanne, Station 6, CH-1015 Lausanne, Switzerland.*

E-mail: hubert.girault@epfl.ch

[b] *Department of Chemistry, Institute of Biomedical Sciences, Fudan University, Shanghai, 200433, P.R. China*

Table of Content

S-1: CHEMICALS EMPLOYED IN THE EXPERIMENTS. 2

S-2: MICROCHIP FABRICATION.....3

S-3: TANDEM MASS SPECTROMETRIC CHARACTERIZATION OF NITRATED ANGIOTENSIN I. 4

S-4: OBSERVED PEAKS ON MASS SPECTRA SHOWN IN FIG. 1 AND FIG. 3. .6

S-5: LEU-ENKEPHALIN AND ALPHA-SYNUCLEIN NITRATION INDUCED BY NITRITE, COPPER(II) AND H_2O_2. 7

S-6: QUANTITATIVE ANALYSIS OF ANGIOTENSIN I AND NITRATED ANGIOTENSIN I BY ESI-MS. 9

S-7: NITRATION INDUCED BY NITRITE, COPPER(II) AND H_2O_2 UNDER DIFFERENT REACTION TIMES. 12

S-8: CHARACTERIZATION OF HYDROXYL RADICAL GENERATION FROM COPPER(II) AND H_2O_2. 14

S-9: TANDEM MASS SPECTROMETRIC CHARACTERIZATION OF ANGIOTENSIN I BOUND COPPER(II). 18

S-10: ON-LINE NITRATION OF 4-AMINOPHENOL INDUCED BY NITRITE, COPPER(II) AND H_2O_2. 20

S-1: Chemicals employed in the experiments.

Angiotensin I (H−DRVYIHPFHL−OH, 98%, Trifluoroacetate salt), β-amyloid 16 (Aβ-16) peptide (H−DAEFRHDSGYEVHHQK−OH) and leu-enkephalin (H−YGGFL−OH) were obtained from Bachem (Switzerland). α-synuclein (107-140) (90%, human, H−APQEGILEDMPVDPDNEAYEMPSEEGYQDYEPEA−OH) was synthesized by the Laboratoire de neurobiologie moléculaire et neuroprotéomique of Ecole Polytechnique Fédérale de Lausanne. Nitrated angiotensin I (H−DRVY(nitro)IHPFHL−OH, 98%) was purchased from Eurogentec (Belgium). Heme was obtained from ABCR (Germany). Iron(II) sulfate ($FeSO_4 \cdot 7H_2O$, 99.5%) and acetic acid (99.8%) were purchased from Merck. Copper(II) chloride ($CuCl_2 \cdot 2H_2O$) was obtained from Acros. Iron(III) chloride ($FeCl_3$, 97%), sodium nitrite ($NaNO_2$, 99%), 4-aminophenol and 1,4,8,11-tetraazacyclotetradecane were obtained from Fluka. Diethylamine NONOate sodium salt hydrate was purchased from Sigma. Hydrogen peroxide (3 WT.% solution in water) was purchased from Sial. Electrador carbon conductor paste (carbon ink) was purchased from Electra Polymer & Chemicals Ltd. UK. Methanol (HPLC grade) was purchased from Applichem. All these reagents were used as received without further purification. Deionized water (18.2 MΩ cm) was obtained from an ultra-pure water system (Milli-Q 185 Plus, Millipore) and used for all experiments.

S-2: Microchip fabrication

Microchips were fabricated using scanning laser ablation. The electrode was made by drilling an L-shape microchannel on a polyimide (PI) substrate (120 μm thickness), Scheme S-2. The L-microchannel was then filled with carbon ink. In a second step, another microchannel was drilled on the same side of the polymer to cross the electrode. At one end of the channel, a reservoir was drilled as a microchannel inlet by static laser drilling. This procedure was repeated to fabricate an array of microchannels. Finally, the PI substrate was laminated with 25/10 μm PE/PET (polyethylene/polyethylene terephthalate) composite sheets (Morane, Oxone, UK), where PE acts as a sealing agent when rolled at 130 °C and 3 bars for 3 s. To insure a good lamination, the entire structure was additionally cured for 1 h at 80 °C. Before use, the tip of the microchannel was cut in a V-shape to facilitate electrospray ionization. The electrode is present at the tip of channel A just before the Taylor cone to supply voltage. The depths and widths of all microchannels are 50 μm and 100 μm, respectively.

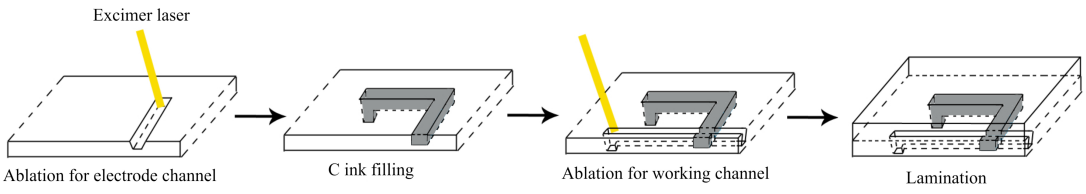

Scheme S-2. Schematic illustration of the fabrication of a polyimide microchip with one micro-channel and one micro-carbon-electrode.

S-3: Tandem mass spectrometric characterization of nitrated angiotensin I.

To identify the structure of nitrated angiotensin I (Ang I), collision induced dissociation (CID) tandem mass spectrometry method was employed. The ion of triple times protonated nitrated Ang I with *m*/*z* of 447.9 Th was selected as parent ion. The fragmentation pattern is shown in Fig. S-3.1. As observed from the mass spectrum, *b*-fragments were nitrated from b_4, while no nitrated *y*-fragments could be observed till y_6. This fragmentation information indicated that the fourth amino acid in this sequence was nitrated. To further demonstrate the structure of the on-line generated nitrated Ang I, the same CID fragmentation was performed on a synthesized peptide of Ang I with nitrated tyrosine, Fig. S-3.2. It was found that the fragmentation pattern of the synthesized nitrated Ang I was same as that of the on-line generated nitrated Ang I, further demonstrating that only tyrosine was nitrated during the on-line nitration process.

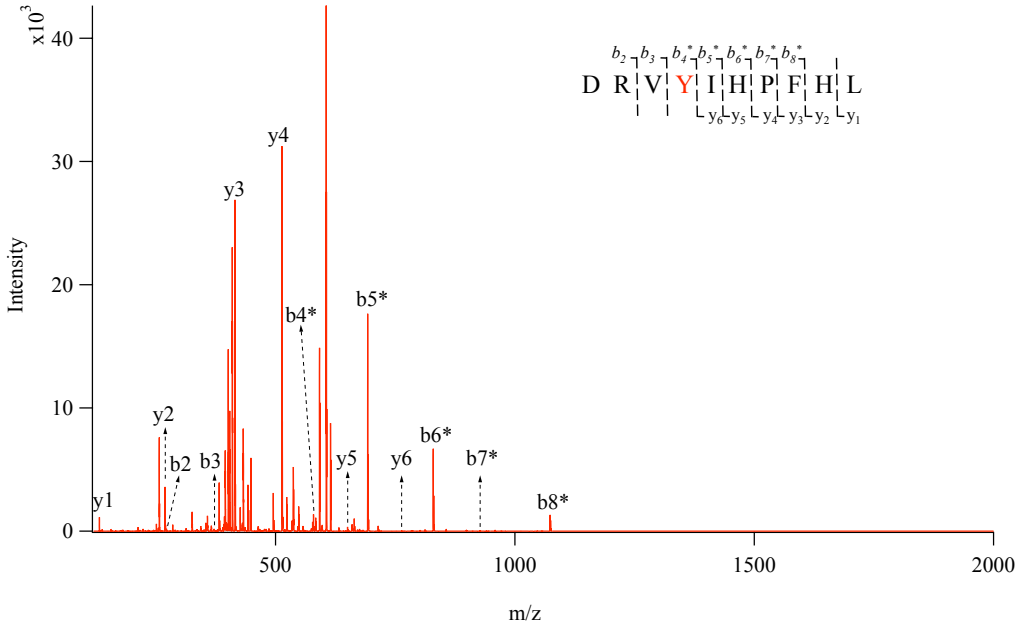

Figure S-3.1. Tandem mass spectrum of the on-line generated nitrated Ang I. The selected parent ion is at *m*/*z* = 447.9 Th ± 1.0 Th. The CID was performed with 20% of instrumental collision energy. *: nitrated fragments.

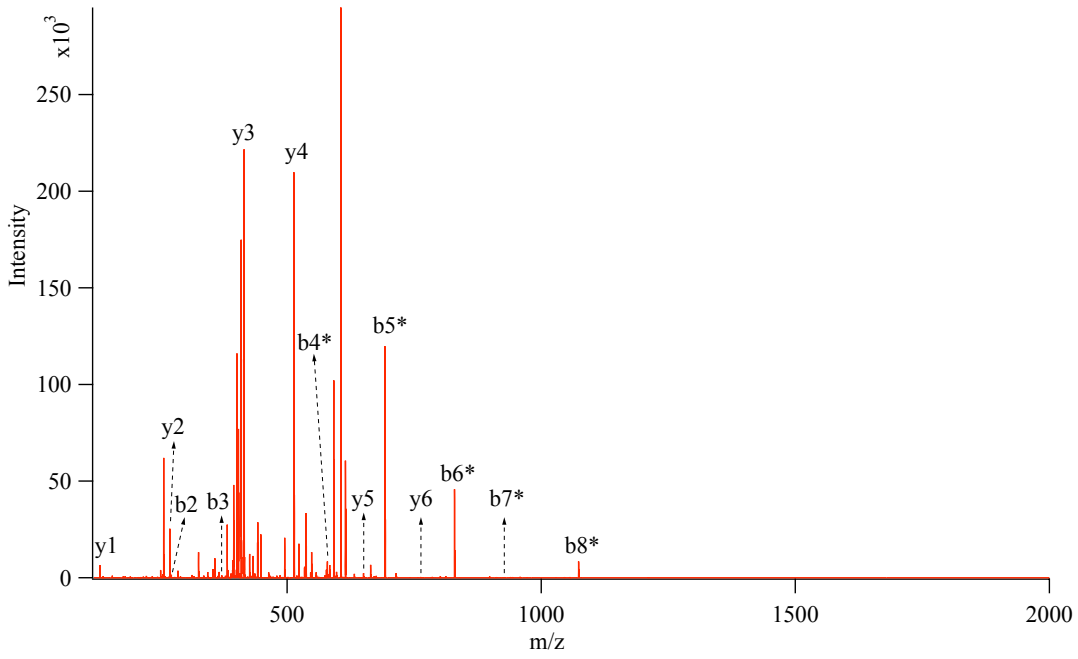

Figure S-3.2. Tandem mass spectrum of the synthesized nitrated Ang I. The selected parent ion is at *m*/*z* = 447.9 Th ± 1.0 Th. The CID was performed with 20% of instrumental collision energy. *: nitrated fragments.

S-4: Observed peaks on mass spectra shown in Fig. 1 and Fig. 3.

Table S-4. Observed peaks on the mass spectra.

Ion	Label	Monoisotopic m/z
3 protonated angiotensin I	$(\text{Ang I})^{3+}$	432.9
2 protonated angiotensin I	$(\text{Ang I})^{2+}$	648.8
3 protonated nitrated angiotensin I	$(NO_2\text{−Ang I})^{3+}$	447.9
2 protonated nitrated angiotensin I	$(NO_2\text{−Ang I})^{2+}$	671.3
3 protonated oxidized angiotensin I	$(\text{O−Ang I})^{3+}$	438.2
1 protonated copper(II)-binding angiotensin I	$(\text{Cu(II)−Ang I})^{3+}$	453.2

S-5: Leu-enkephalin and Alpha-synuclein nitration induced by nitrite, copper(II) and H_2O_2.

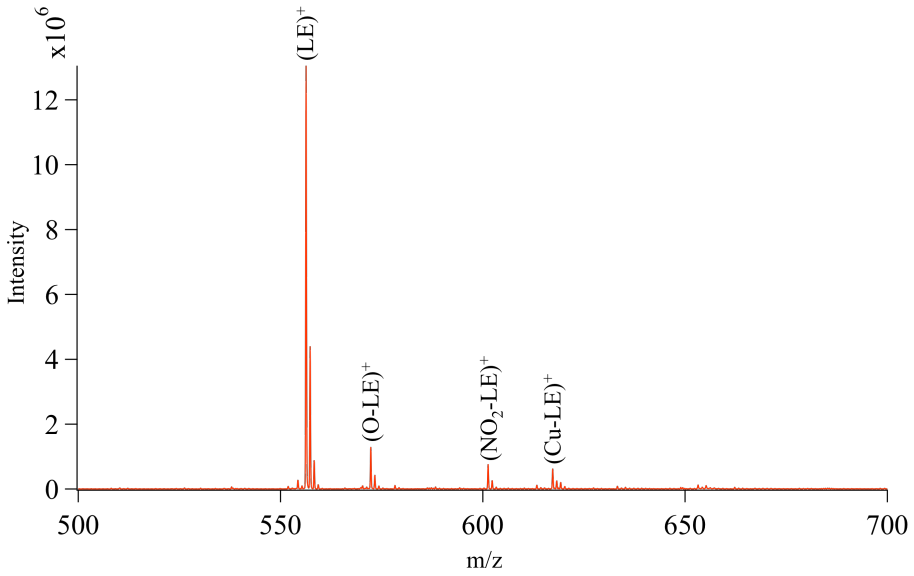

Figure S-5.1. Mass spectrum of leu-enkephalin (LE) on-line nitration products. The nitration was performed in the microchip with flow rates in channel A and B of 0.05 $\mu l \cdot min^{-1}$ and a flow rate in channel C of 1 $\mu l \cdot min^{-1}$. Channel A: 0.5 mM of LE, 1 mM of H_2O_2 and 2 mM of $NaNO_2$ in H_2O; channel B: 0.5 mM of $CuCl_2$ in H_2O; channel C: ESI buffer. Oxidized LE (O−LE), nitrated LE (NO_2−LE) and copper(II)-binding LE with the loss of one proton (Cu−LE) were observed.

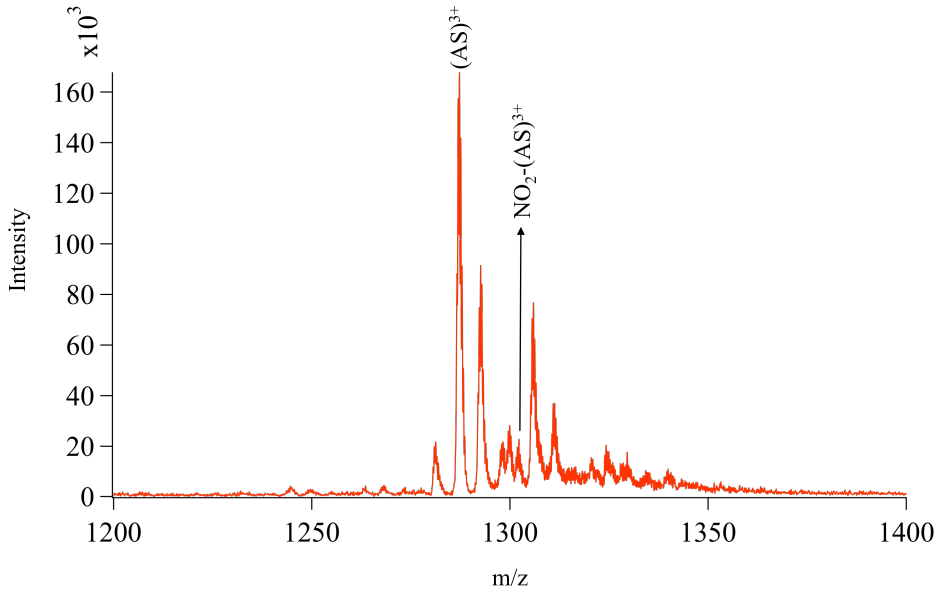

Figure S-5.2. Mass spectrum of human α-synuclein fragment (107-140) (AS) on-line nitration products. The nitration was performed in the microchip with flow rates in channel A and B of 0.05 μl·min^{-1} and a flow rate in channel C of 1 μl·min^{-1}. Channel A: 0.5 mM of AS, 1 mM of H_2O_2 and 2 mM of $NaNO_2$ in H_2O; channel B: 0.5 mM of $CuCl_2$ in H_2O; channel C: ESI buffer. Nitrated AS (NO_2−AS) can be observed on the mass spectrum. The other observed peaks are generated mainly from the contaminants in the synthesized α-synuclein fragment (107-140).

S-6: Quantitative analysis of angiotensin I and nitrated angiotensin I by ESI-MS.

An external standard calibration method was employed for quantitatively analyzing the generation of NO_2−Ang I. Typically, synthesized NO_2−Ang I was mixed with unmodified Ang I under different ratios in the ESI buffer. The mixtures were analyzed by either microchip ESI-MS or commercial source ESI-MS. In the case of microchip ESI-MS, a three-channel microchip similar as the one shown in Scheme 1 with a carbon electrode placed in channel A was used as an emitter. Channel A of the three-channel microchip was used to introduce samples. Channel B and C were blocked during the experiments. Intensities of the peaks at *m*/*z* of 432.9 Th (P_2) and 447.9 Th (P_1) were read out for calibration. $P_1/(P_1+P_2)$ was plotted as a function of $M_1/(M_1+M_2)$ to obtain a calibration curve, where M_1 is the concentration of NO_2−Ang I and M_2 is the concentration of Ang I. Each experiment was repeated several times to calculate the average values of $P_1/(P_1+P_2)$ and the standard deviation.

Fig. S-6a and b show the calibration curves obtained under the conditions of $M_1 + M_2 = 41.6$ μM and 1.2 μl·min^{-1} of flow rate by using microchip ESI. This calibration curve was specially obtained for the quantification of NO_2−Ang I on-line generated when the flow rates in channel A and B are 0.1 μl·min^{-1} and the flow rate in channel C is 1 μl·min^{-1}, where the final flow rate for ESI is 1.2 μl·min^{-1} and the final summed concentration of nitrated and unmodified Ang I is 41.6 μM. Good linearity was found under a wide range of $M_1/(M_2+M_1)$ from 0.0125 to 0.5, Fig. S-6a. The trendline was also obtained between 0.0125 and 0.075 of $M_1/(M_2+M_1)$, Fig. S-6b.

Calibration curve shown in Fig. S-6c was employed to quantify the NO_2−Ang I on-line generated under flow rates in channel A and B of 0.05 μl·min^{-1} and the flow

rate in channel C of 1 μl·min^{-1}. This calibration curve was also used to quantify the off-line generated NO_2−Ang I that was identified by microchip ESI-MS under the flow rate in channel A of 1.1 μl·min^{-1}. Calibration curve shown in Fig. S-6d was employed to quantify the off-line generated NO_2−Ang I that was identified by commercial source ESI-MS under the flow rate of 10 μl·min^{-1}. Considering the good linearity of the trendlines and small values of standard deviation, both microchip ESI-MS and commercial source ESI-MS can be used to quantitatively analyze the generation of NO_2−Ang I.

In the presence of $NaNO_2$ and $CuCl_2$ with concentrations as high as 10 mM, the protonated peaks still dominated the mass spectra because the used ESI buffer was very acidic, and the corresponding nitration level could still be calculated by using the same calibration curves.

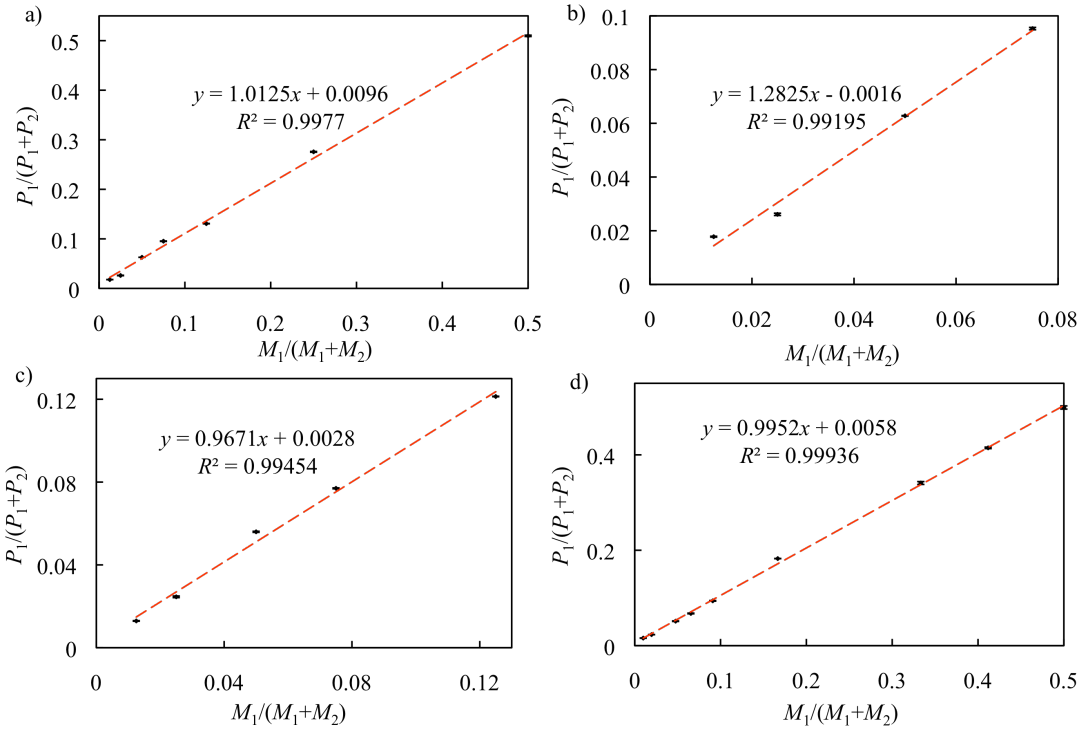

Figure S-6. Calibration curves in the range of a) 0.0125 to 0.5 of $M_1/(M_1+M_2)$ and b) 0.0125 to 0.075 of $M_1/(M_1+M_2)$ for the quantification of Ang I nitration level obtained under the conditions of $M_1 + M_2$ = 41.6 μM and 1.2 μl·min^{-1} of flow rate by using microchip ESI. c) Calibration curve for the

quantification of Ang I nitration level obtained under the conditions of $M_1 + M_2 = 22.7$ μM and 1.1 μl·min^{-1} of flow rate by using microchip ESI. d) Calibration curve for the quantification of Ang I nitration level obtained under the conditions of $M_1 + M_2 = 22.7$ μM and 10 μl·min^{-1} of flow rate by using commercial source ESI. The error bars in the figures show the standard deviation of $P_1/(P_1+P_2)$.

S-7: Nitration induced by nitrite, copper(II) and H_2O_2 under different reaction times.

The nitration with a reaction time of 0.5 min or 1 min was performed on-line in the microchip, while the nitration with a reaction time of 4 hours was performed off-line and analyzed by microchip ESI-MS. The reaction time for on-line nitration was calculated by considering the flow rates and the total volume of the reaction region. Because methanol is a strong radical scavenger, the nitration should mainly happen after the mixing of the solutions in channel A and B but before the introduction of ESI buffer, in a 2 cm long reaction region in the channel A. The reaction volume can then be calculated as 2 cm × 50 μm × 100 μm by considering the structure of the microchip shown in Scheme 1. With the flow rates in channel A and B of 0.1 $\mu l \cdot min^{-1}$, the reaction time is 0.5 min. With the flow rates in channel A and B of 0.05 $\mu l \cdot min^{-1}$, the reaction time is 1 min. The nitration level was calculated from $P_1/(P_1+P_2)$ by using the calibration curves shown in Fig. S-6b and c. Each experiment was repeated several times to calculate the average nitration levels and the standard deviation.

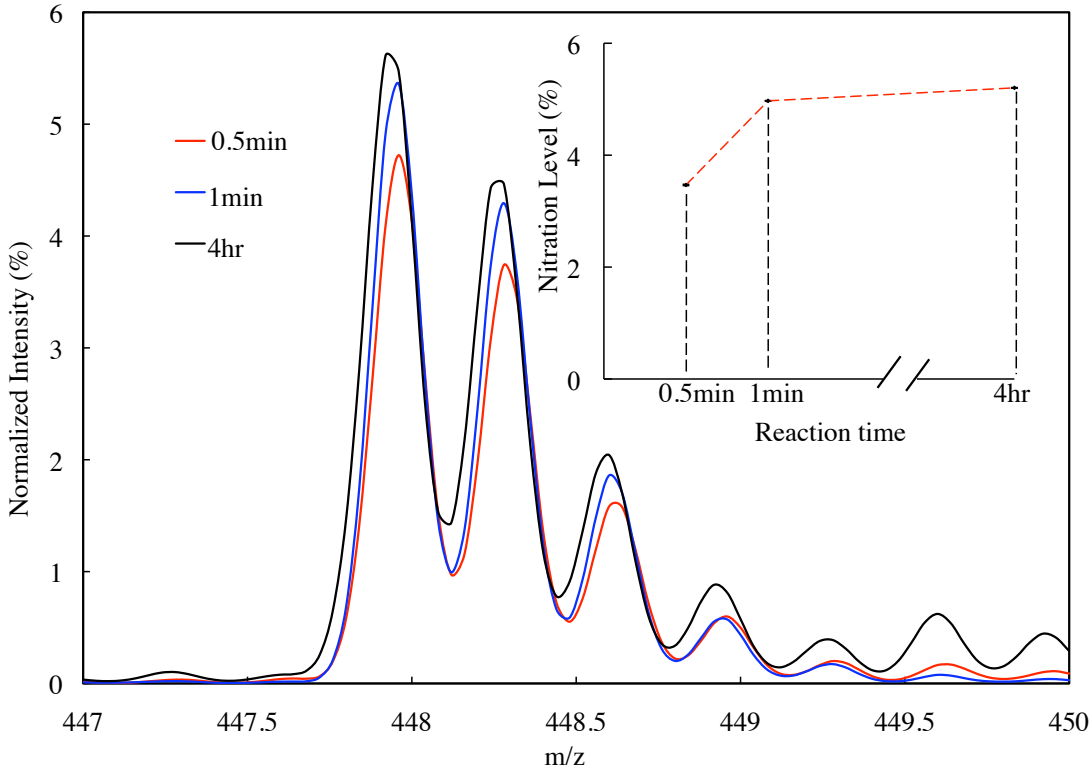

Figure S-7. Ang I nitration under varied reaction times. The experimental conditions for on-line reaction: flow rate in channel C: 1 μl·min^{-1}; solution in channel A: 0.5 mM of Ang I, 1 mM of H_2O_2 and 2 mM of $NaNO_2$ in H_2O; solution in channel B: 0.5 mM of $CuCl_2$ in H_2O; solution in channel C: ESI buffer. Mass spectra are normalized by setting the monoisotopic peak intensities of $(Ang\ I)^{3+}$ always as 100%. The calculated nitration level is plotted against reaction time in Fig. S-7 inset. The error bars in the figures show the standard deviation of nitration level.

S-8: Characterization of hydroxyl radical generation from copper(II) and H_2O_2.

Here, the characterized hydroxyl radical can be a sum of diffusible and copper(II)-bound hydroxyl radical. For simplification, the •OH radical mentioned in this section indicates both diffusible and copper(II)-bound hydroxyl radicals.

In the absence of nitrite, the produced •OH radical would mainly be scavenged by terephthalic acid (TA) to generate 2-hydroxyterephthalic acid (OHTA), and therefore the overall reactions can be expressed as:

$$\begin{aligned} &CuCl_2 + H_2O_2 \xrightarrow{k_2} {}^{\bullet}OH \\ &{}^{\bullet}OH + TA \xrightarrow{k_1} OHTA \end{aligned} \qquad (1)$$

Considering a steady state for the generation of •OH radical, the OHTA generation kinetics can be written as:

$$\begin{aligned} &\frac{\mathrm{d}F}{\mathrm{d}t} = \eta \frac{\mathrm{d}[C_{\mathrm{OHTA}}]}{\mathrm{d}t} \\ &\frac{\mathrm{d}[C_{\mathrm{OHTA}}]}{\mathrm{d}t} = k_1[C_{\bullet\mathrm{OH}}][C_{\mathrm{TA}}] \\ &\frac{\mathrm{d}[C_{\bullet\mathrm{OH}}]}{\mathrm{d}t} = k_2[C_{\mathrm{H_2O_2}}]^a[C_{\mathrm{CuCl_2}}]^b - k_1[C_{\bullet\mathrm{OH}}][C_{\mathrm{TA}}] - k_{\mathrm{S}}[C_{\bullet\mathrm{OH}}][C_{\mathrm{S}}] = 0 \end{aligned} \qquad (2)$$

where F is the fluorescence intensity; η is a constant depending on the instrumental parameters of fluorescence spectrometer; [C] is the concentration of the different species; a & b are apparent reaction rate orders with respect to H_2O_2 & $CuCl_2$, respectively; S represents globally any scavenger other than TA. The last equation represents the steady state approximation applied to the •OH radical.

According to Fig. 5, the fluorescence intensity of the reaction product of H_2O_2, $CuCl_2$ and terephthalic acid is proportional to the reaction time, either indicating that

the reactions are pseudo zeroth-order or indicating that the concentrations of reactants do not vary much in 60 min of reaction. Considering the complex mechanism for $^{\bullet}OH$ radical generation shown in Scheme 2, the second possibility is more reasonable.

In the presence of nitrite, $^{\bullet}OH$ radical would be scavenged by both TA and nitrite, and the overall reactions can be expressed as:

$$\begin{aligned} &CuCl_2 + H_2O_2 \xrightarrow{k_2} {}^{\bullet}OH \\ &{}^{\bullet}OH + TA \xrightarrow{k_1} OHTA \\ &{}^{\bullet}OH + NO_2^- \xrightarrow{k_3} {}^{\bullet}NO_2 \end{aligned} \qquad (3)$$

The steady state approximation now reads:

$$\frac{\mathrm{d}\left[C_{\bullet OH}\right]_2}{\mathrm{d}t} = k_2\left[C_{H_2O_2}\right]^a\left[C_{CuCl_2}\right]^b - k_1\left[C_{\bullet OH}\right]_2\left[C_{TA}\right] - k_S\left[C_{\bullet OH}\right]_2\left[C_S\right] - k_3\left[C_{\bullet OH}\right]_2\left[C_{nitrite}\right] = 0 \qquad (4)$$

where $[C_{\bullet OH}]_2$ is the concentration of $^{\bullet}OH$ in the presence of nitrite. According to the slopes shown in Fig. 5, dF/dt is equal to 3.12 and 0.93 (a.u·min^{-1}) in the absence and presence of nitrite.

From equations (2) & (4), we have

$$\frac{\mathrm{d}F}{\mathrm{d}t} = \eta\frac{\mathrm{d}\left[C_{OHTA}\right]}{\mathrm{d}t} = \eta k_1\left[C_{\bullet OH}\right]\left[C_{TA}\right] = 3.12 \qquad (5)$$

$$\frac{\mathrm{d}F_2}{\mathrm{d}t} = \eta\frac{\mathrm{d}\left[C_{OHTA}\right]_2}{\mathrm{d}t} = \eta k_1\left[C_{\bullet OH}\right]_2\left[C_{TA}\right] = 0.93 \qquad (6)$$

$$\begin{aligned} \frac{\mathrm{d}F}{\mathrm{d}t} &= \eta\frac{\mathrm{d}\left[C_{OHTA}\right]}{\mathrm{d}t} = \eta\left(k_2\left[C_{H_2O_2}\right]^a\left[C_{CuCl_2}\right]^b - k_S\left[C_S\right]\left[C_{\bullet OH}\right]\right) \\ &= \eta k_2\left[C_{H_2O_2}\right]^a\left[C_{CuCl_2}\right]^b - \frac{3.12k_S\left[C_S\right]}{k_1\left[C_{TA}\right]} = 3.12 \end{aligned} \qquad (7)$$

$$\frac{\mathrm{d}F_2}{\mathrm{d}t} = \eta\frac{\mathrm{d}\left[C_{\mathrm{OHTA}}\right]_2}{\mathrm{d}t} = \eta\left(k_2\left[C_{\mathrm{H_2O_2}}\right]^a\left[C_{\mathrm{CuCl_2}}\right]^b - k_{\mathrm{S}}\left[C_{\bullet\mathrm{OH}}\right]_2\left[C_{\mathrm{S}}\right] - k_3\left[C_{\bullet\mathrm{OH}}\right]_2\left[C_{\mathrm{nitrite}}\right]\right)$$
$$= \eta k_2\left[C_{\mathrm{H_2O_2}}\right]^a\left[C_{\mathrm{CuCl_2}}\right]^b - \frac{0.93\left(k_{\mathrm{S}}\left[C_{\mathrm{S}}\right] + k_3\left[C_{\mathrm{nitrite}}\right]\right)}{k_1\left[C_{\mathrm{TA}}\right]} = 0.93 \quad (8)$$

From equations (5) & (6), we have $[C_{\bullet\mathrm{OH}}]_2 = 29.8\%[C_{\bullet\mathrm{OH}}]$, indicating that 70.2% of $^{\bullet}$OH radicals generated are scavenged by nitrite.

By subtracting equation (8) from equation (7) and assuming that the concentrations of the reactants do not vary, we have

$$0.93k_3\left[C_{\mathrm{nitrite}}\right] = 2.19\left(k_1\left[C_{\mathrm{TA}}\right] + k_{\mathrm{s}}\left[C_{\mathrm{s}}\right]\right) \quad (9)$$

Considering that the $^{\bullet}$OH radical would mainly be scavenged by terephthalic acid in the absence of nitrite, we have $k_{\mathrm{s}}[C_{\mathrm{s}}] << k_1[C_{\mathrm{TA}}]$. Then equation (9) can be simplified as:

$$\frac{k_1\left[C_{\mathrm{TA}}\right]}{k_3\left[C_{\mathrm{nitrite}}\right]} = \frac{0.93}{2.19} \quad (10)$$

and considering the concentrations used ($[C_{\mathrm{TA}}]$ = 0.1 mM and ($[C_{\mathrm{nitrite}}]$ = 3 mM), we have k_3 = 7.8%k_1. Therefore, nitrite is an efficient $^{\bullet}$OH scavenger holding a scavenging rate constant 7.8% that of terephthalic acid.

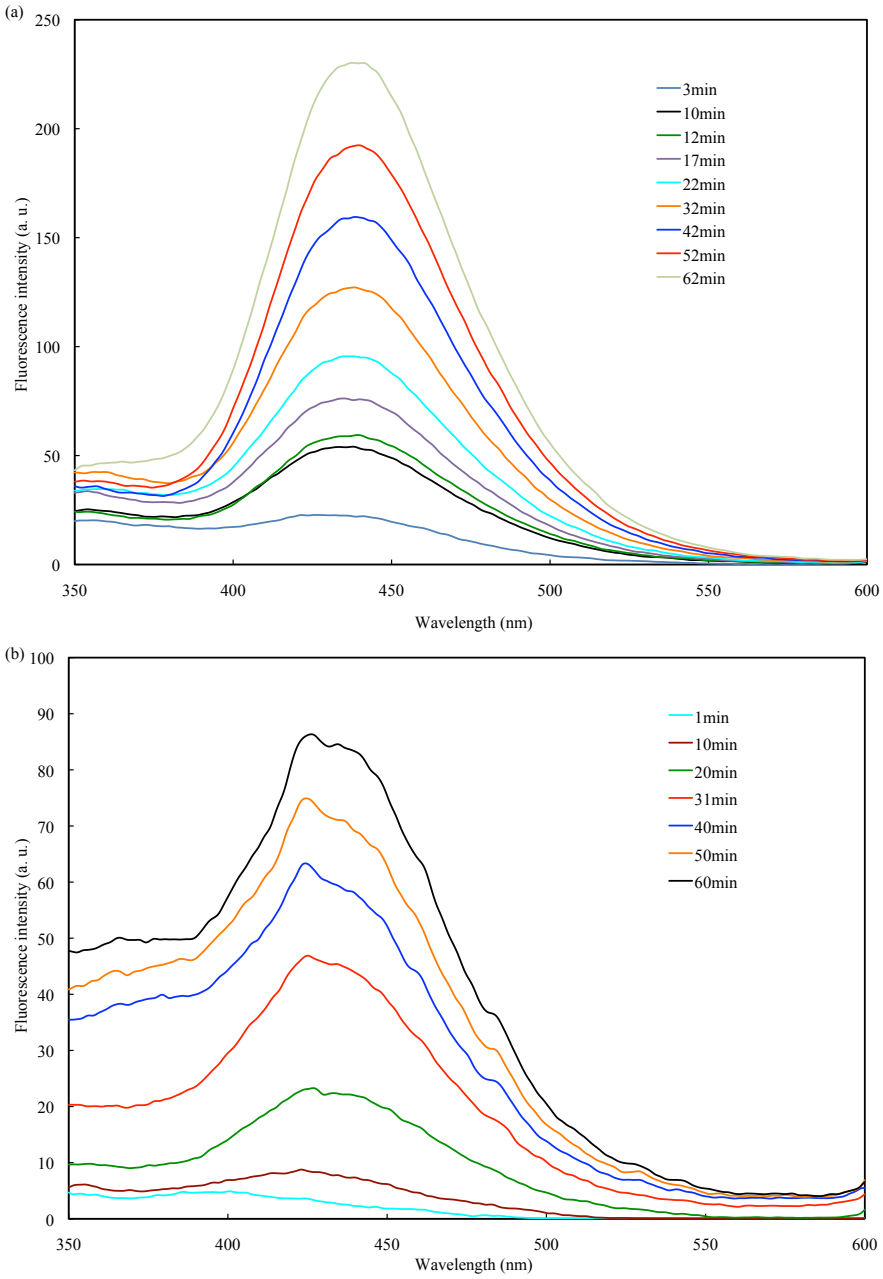

Figure S-8. Fluorescence spectra of the reaction products of H_2O_2 (3 mM), $CuCl_2$ (3 mM) and terephthalic acid (0.1 mM, saturated aqueous solution) (a) without or (b) with $NaNO_2$ (3 mM). Reaction time is shown on the figure.

S-9: Tandem mass spectrometric characterization of angiotensin I bound copper(II).

The ion of (Cu(II)-Ang I)$^{3+}$ with *m/z* of 453.2 Th was selected as parent ion. The fragmentation pattern is shown in Fig. S-9.1. Because of the observation of copper-binding b_6 fragment, Cu^{2+} should be located in the sequence from D to H. Considering that both a_3 and y_7 fragments were observed without the appearance of copper (II) ion, the Cu^{2+} may be located on the carbonyl group of the backbone between valine and tyrosine. To further demonstrate the hypothesis, the $(b_6^*)^{2+}$ fragment on Fig. S-9.1 was selected as parent ion to run MS^3 fragmentation. As shown in Fig. S-9.2, fragments of b_3, c_3 and y_4 were observed to bind the copper (II) ion, illustrating that the Cu^{2+} should be located on the residue of valine or the carbonyl group of the backbone between valine and tyrosine. Considering that the side-chain of valine only consists of alkyl, the latter possibility is more reasonable.

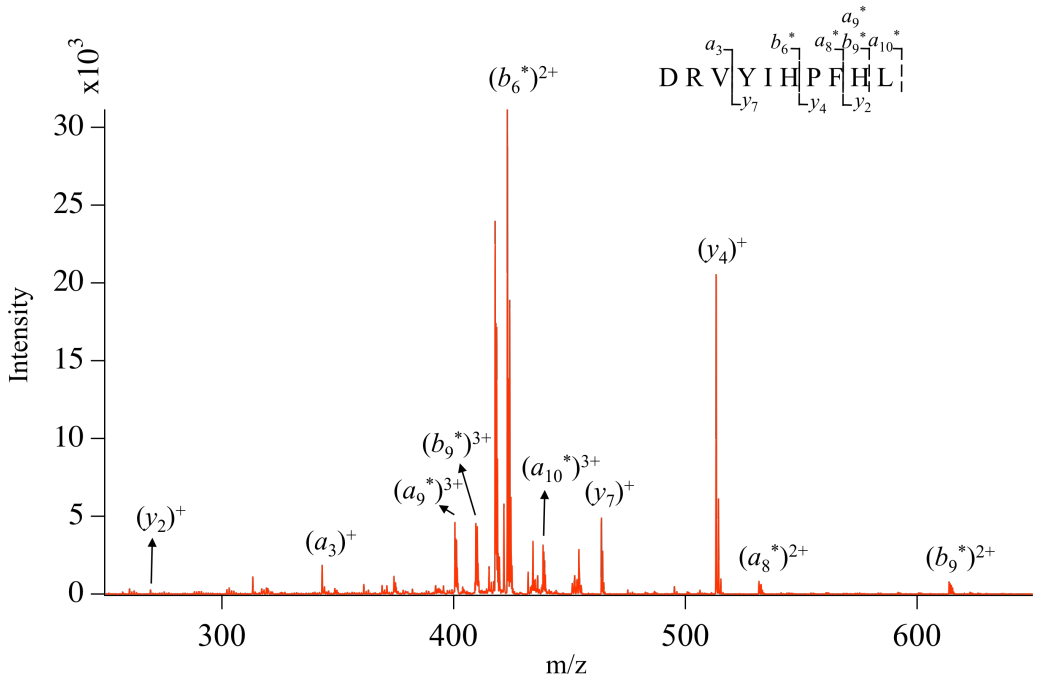

Figure S-9.1. Tandem mass spectrum of (Cu(II)-Ang I)$^{3+}$. The selected parent ion is at m/z = 453.2 Th ± 2.0 Th. The CID was performed with 20% of instrumental collision energy. *: Copper-binding fragments.

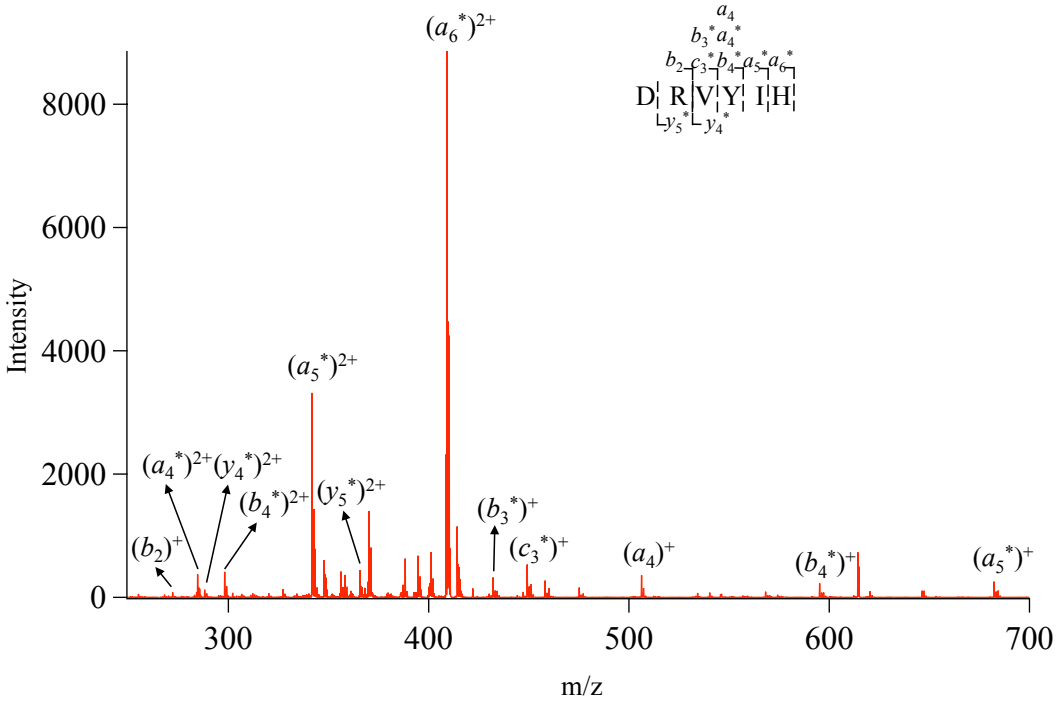

Figure S-9.2. Tandem mass spectrum of the $(b_6^*)^{2+}$ fragment on Fig. S-9.1. The selected parent ion is at m/z = 423.2 Th ± 2.0 Th. The CID was performed with 20% of instrumental collision energy. *: Copper-binding fragments.

S-10: On-line nitration of 4-aminophenol induced by nitrite, copper(II) and H_2O_2.

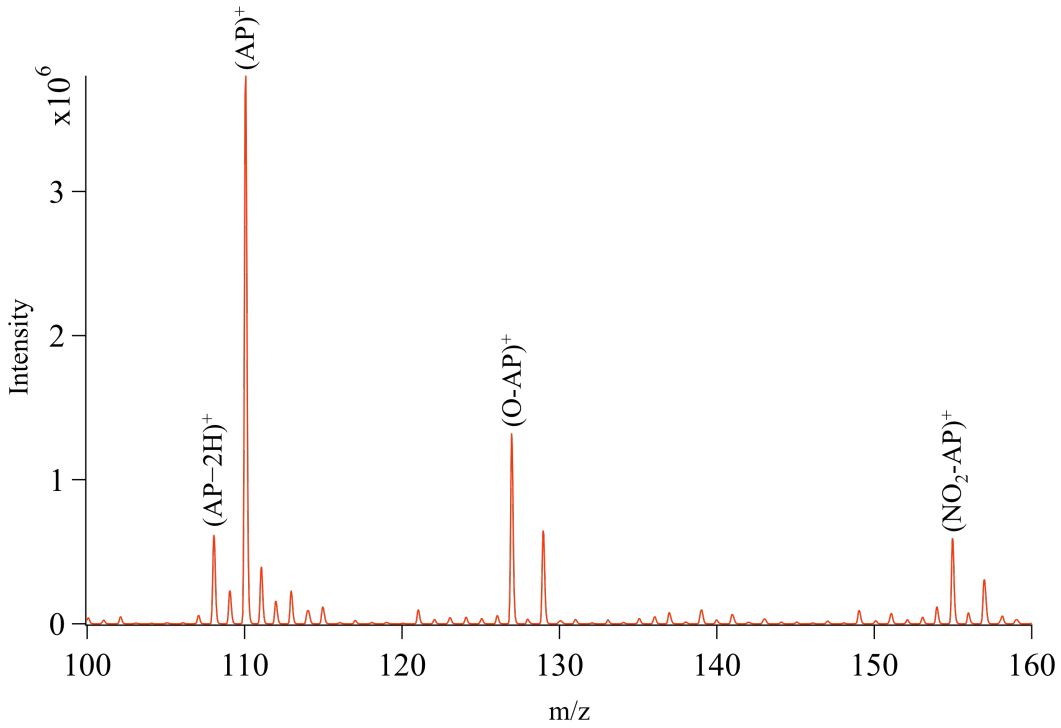

Figure S-10. Mass spectrum of 4-aminophenol (AP) on-line nitration products. The nitration was performed in the microchip with flow rates in channel A and B of 0.05 μl·min^{-1} and a flow rate in channel C of 1 μl·min^{-1}. Channel A: 5 mM of AP, 2 mM of H_2O_2 and 2 mM of $NaNO_2$ in H_2O; channel B: 5 mM of $CuCl_2$ in H_2O; channel C: ESI buffer. Nitrated AP can be observed on the mass spectrum together with the oxidized AP. Because the AP is more difficult than peptides to be ionized, concentrated AP was used to perform ESI-MS.